Advances in Applied Mathematics and Mechanics
Adv. Appl. Math. Mech., Vol. **1**, No. 2, pp. 151-165 (2009)

April 2009

Viscoelastic Models for Passive Arterial Wall Dynamics

D. Valdez-Jasso[1], H. T. Banks[1], M.A. Haider[1], D. Bia[2], Y. Zocalo[2], R. L. Armentano[2,3] and M. S. Olufsen[1,*]

[1] *Department of Mathematics and Center for Research in Scientific Computation, NC State University, Campus Box 8205, Raleigh, NC 27695*

[2] *Departmento de Fisiologia, Facultad de Medicina, Universidad de La Republica, General Flores 2125, PC: 11800, Montevideo, Uruguay*

[3] *Facultad de Ingenieria y Ciencias Exactas y Naturales, Universidad Favaloro, Avda. Belgrano 1723, Capital Federal, Buenos Aires, Argentina*

Received 13 December 2008; Accepted (in revised version) 16 January 2009

Available online 17 March 2009

Abstract. This paper compares two models predicting elastic and viscoelastic properties of large arteries. Models compared include a Kelvin (standard linear) model and an extended 2-term exponential linear viscoelastic model. Models were validated against in-vitro data from the ovine thoracic descending aorta and the carotid artery. Measurements of blood pressure data were used as an input to predict vessel cross-sectional area. Material properties were predicted by estimating a set of model parameters that minimize the difference between computed and measured values of the cross-sectional area. The model comparison was carried out using generalized analysis of variance type statistical tests. For the thoracic descending aorta, results suggest that the extended 2-term exponential model does not improve the ability to predict the observed cross-sectional area data, while for the carotid artery the extended model does statistically provide an improved fit to the data. This is in agreement with the fact that the aorta displays more complex nonlinear viscoelastic dynamics, while the stiffer carotid artery mainly displays simpler linear viscoelastic dynamics.

AMS subject classifications: 74D05, 74J25, 62J02, 93A30,92C10, 74L15

Key words: Arterial wall modeling, dynamic viscoelastic models, inverse problems, statistical analysis for model comparison.

*Corresponding author.
URL: `http://www4.ncsu.edu/~msolufse/`
Email: dvaldez@ncsu.edu (D. Valdez-Jasso), htbanks@ncsu.edu (H. T. Banks), mahaider@ncsu.edu (M.A. Haider), dbia@fmed.edu.uy (D. Bia), yana@fmed.edu.uy (Y. Zocalo), armen@ieee.org (R. L. Armentano), msolufse@ncsu.edu (M. S. Olufsen)

1 Introduction

The arterial walls of the cardiovascular system are known to display complex mechanical responses under physiological conditions. The typical arterial wall consists of three layers: an innermost layer, "the intima", mainly composed of endothelial cells, a middle layer, "the media", composed of elongated smooth muscle cells, elastin and collagen, and an outer layer "the adventitia" comprising a varied number of elastic sheets, bundles of collagen fibrils, and a network of elastic fibrils. These layers and the composition of the layers are shown in Fig. 1.

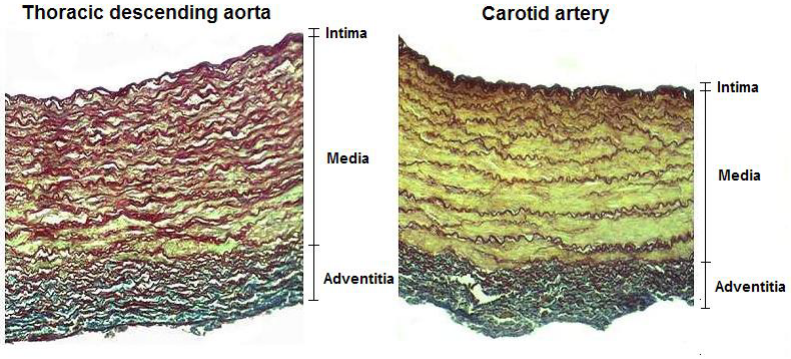

Figure 1: Histological slices displaying a cross section of the arterial wall for the thoracic descending aorta (left) and the carotid artery (right) from ovine arteries. The vessels were stained with orcein using the Cajal-Gallengo method, which allows discrimination of the three main wall components that determine the arterial biomechanical behavior: smooth muscle cells (yellow), elastin (dark red), and collagen (blue). Note that the carotid artery has a higher proportion of smooth muscle cells ($\approx 60\%$) than the thoracic descending aorta ($\approx 40\%$), while the aorta has more elastin fibers than the carotid artery.

In this study, our focus is on viscoelastic modeling of the passive dynamic mechanical responses of the arterial wall under in-vitro conditions that mimic in-vivo physiological conditions. Within this context, two models will be evaluated by comparison to experimental pressure-area data for two arteries: the thoracic descending aorta and the carotid artery. The aorta is the largest artery in the cardiovascular system while the carotid artery is significantly smaller. For sheep arteries, the thoracic descending aorta typically has a diameter of 2 cm, while the carotid artery has a diameter of approximately 0.8 cm. The collagen-elastin-smooth muscle cell composition of these two types of arteries is different; the aorta contains a significant amount of elastin fibers and fewer smooth muscle cells (approximately 40% of the aortic vessel wall is composed of smooth muscle cells), while the carotid artery has less elastin and significantly more smooth muscle cells (approximately 60%) [15]. Another difference between the two vessels is that the separation between elastin fibers, collagen fibers, and smooth muscle cells are more distinguished for the carotid artery than for the aorta; see Fig. 1.

For both vessels, the media layer gives rise to the majority of the vessel's viscoelastic behavior, and it is the presence and organization of fibers and smooth muscle cells

that allow the arteries to stretch while, simultaneously, inhibiting over-expansion due to fluid pressure exerted on the vessel walls by the blood flow [16, 20, 23], preventing their rupture.

Viscoelastic responses are evidenced via the presence of hysteresis-like loops in parametric plots of pressure-area data. Many models have been developed to study the mechanical properties of the systemic arteries, but few studies have been validated against in-vitro data designed to mimic arterial wall deformation under in-vivo physiological conditions. For a recent review discussing previous modeling approaches see Kassab [14].

Quasilinear viscoelasticity (QLV) theory has been widely used to characterize the viscoelastic mechanics of biological soft tissues [11, 13, 24]. In large part, the success of QLV theory in this context is based on its ability to tailor both the viscoelastic relaxation function and the nonlinear elastic stress-strain response to observed mechanical responses for the specific soft tissue of interest. The Fung-type continuous spectrum relaxation function [11] has seen wide usage due to its consistency with the relatively rate-insensitive response of many soft tissues to dynamical mechanical loading over a range of frequencies, see e.g., [24]. However, numerical evaluation of the associated continuous spectrum integral can be tedious and, consequently, a common remedy is to re-approximate the relaxation function using a few terms of an exponential series or a model with a finite number of relaxation terms that in the limit approaches a model with a continuum relaxation spectrum [5–7].

The goal of this study is to predict mechanical properties of the arterial wall. We predict these properties by solving an inverse problem. Mechanical properties are extracted from model parameters by solving a nonlinear least squares problem minimizing the difference between model computed and measured values of cross-sectional area. We will compare two linear viscoelastic relaxation models formulated to relate pressure and cross-sectional area dynamics observed in-vitro under physiological flow conditions. The two models studied are the Kelvin (standard linear) model and an extended 2-term exponential series linear viscoelastic model.

2 Models and methods

In this study, blood pressure is treated as an input to the mechanical models which, in turn, are used to simulate deformation of the vessel's cross-sectional area. In this section, we describe the two viscoelastic models, the experimental data employed to solve the inverse problem, and statistical techniques used for analysis and comparison of the models.

2.1 Kelvin viscoelastic model

The Kelvin model can be derived under the assumption that the artery can be idealized as a thin walled tube [12]. We formulate the model by relating vessel strain s and

transmural arterial pressure p mmHg as

$$s(t) + \tau_\sigma \frac{ds}{dt} = \frac{r_0}{Eh}\Big(p + \tau_\epsilon \frac{dp}{dt}\Big), \quad s(t) = \Big(1 - \sqrt{\frac{A_0}{A(t)}}\Big), \tag{2.1}$$

where in our subsequent model $A(t)$ cm^2 is the cross-sectional area of the vessel and $A_0{=}\pi r_0^2$ cm^2 is the zero-pressure area. The material parameters are the zero-pressure radius r_0 cm, the vessel wall thickness h cm, elastic (stiffness) modulus E mmHg, and the viscoelastic relaxation times τ_ϵ sec and τ_σ sec. Since the parameters E and h are linearly dependent, we take the product Eh as one independent parameter, resulting in a total of four independent parameters for the Kelvin model. Note that (2.1) reduces to an elastic model when the relaxation times are set to zero, i.e., for $\tau_\sigma{=}\tau_\epsilon{=}0$.

The Kelvin model is the simplest viscoelastic model that, simultaneously, captures effects of creep, stress relaxation and storage of strain energy at equilibrium. In our previous study [22], material properties $(r_0, Eh, \tau_\sigma, \tau_\epsilon)$ were extracted using nonlinear optimization minimizing the least squares error between measured and computed model values of cross-sectional area, $A(t)$. Model estimates were obtained using $p(t)$ as an input to predict $A(t)$ using (2.1) to relate the quantities.

To avoid numerical differentiation of the pressure data, (2.1) was re-written in an equivalent hereditary integral form, obtained by integrating (2.1) from 0 to t seconds. The resulting integral model is given by

$$\begin{aligned} s(t) = &\left(s(0) - \frac{r_0}{Eh}\frac{\tau_\epsilon}{\tau_\sigma}p(0)\right) e^{-t/\tau_\sigma} + \frac{r_0}{Eh}\frac{\tau_\epsilon}{\tau_\sigma}p(t) \\ &+ \frac{r_0}{Eh}\frac{\tau_\sigma - \tau_\epsilon}{\tau_\sigma^2}\int_0^t e^{-(t-\gamma)/\tau_\sigma}\, p(\gamma)\, d\gamma. \end{aligned} \tag{2.2}$$

In the context of our application, it is noted that we associate $t{=}0$ with an intermediate state of vessel deformation, as opposed to a zero-strain state. While a zero-strain state can be achieved in-vitro, our modeling approach is to mimic in-vivo conditions, where it is not possible to achieve a zero-strain state.

2.2 Extended viscoelastic model

Refinement of the Kelvin model typically incorporates two extensions. The first is the consideration of nonlinear (finite) strains, while the second is the incorporation of additional relaxation time scales that represent the diverse viscoelastic mechanical response of the constituent fibers of a soft tissue. Fung's quasilinear viscoelasticity (QLV) theory [11] provides a framework within which to develop such models. The QLV representation of viscoelastic models is typically of the form

$$s(t) = \int_{-\infty}^{t} K(t-\gamma)\frac{\partial s^{(e)}[p(\gamma)]}{\partial \gamma} d\gamma, \tag{2.3}$$

where $K(t)$ is a reduced creep function, and the inverse elastic response is specified by a function $s^{(e)}[p]$. In our application, time integration is performed from 0 to t seconds, and the unknown functions in (2.3) for the Kelvin model are

$$s^{(e)}[p] = \frac{r_0}{Eh}p, \qquad K(t) = 1 - \frac{\tau_\sigma - \tau_\epsilon}{\tau_\sigma}e^{-t/\tau_\epsilon}. \tag{2.4}$$

This correspondence is more clearly seen by re-writing (2.2), using integration-by-parts, to obtain

$$\begin{aligned} s(t) &= \left(s(0) - \frac{r_0}{Eh}p(0)\right)e^{-t/\tau_\sigma} + \frac{r_0}{Eh}p(0) \\ &\quad + \frac{r_0}{Eh}\int_0^t \left(1 - \frac{\tau_\sigma - \tau_\epsilon}{\tau_\sigma}e^{-(t-\gamma)/\tau_\sigma}\right)\frac{dp(\gamma)}{d\gamma}d\gamma \\ &= \left(s(0) - \frac{r_0}{Eh}p(0)\right)e^{-t/\tau_\sigma} + \frac{r_0}{Eh}p(0) + \int_0^t K(t-\gamma)\frac{d}{d\gamma}\left(\frac{r_0}{Eh}p(\gamma)\right)d\gamma, \end{aligned} \tag{2.5}$$

where $K(t)$ is as stated in (2.4), and the terms outside the integral arise due to consideration of an intermediate state of vessel deformation at t=0 seconds.

The focus of the current study is the development and analysis of an extended model accounting for additional viscoelastic relaxation times within the confines of the small strain assumption. As such, the first relation in (2.4) will remain the same, while the function $K(t)$ and the terms outside the integral in (2.5) will be modified. We introduce a new creep function $G(t)$ that involves two independent relaxation times by writing

$$G(t) = 1 - A_1e^{-t/b_1} - A_2e^{-t/b_2}, \qquad A_1, A_2 \geq 0 \ \text{ and } \ b_1, b_2 > 0. \tag{2.6}$$

When extending (2.5), we incorporate $G(t)$ both inside and outside the integral. Consider the following model

$$s(t) = \left(s(0) - \frac{r_0}{Eh}p(0)\right)G(t) + \frac{r_0}{Eh}p(0) + \frac{r_0}{Eh}\int_0^t G(t-\gamma)\frac{dp}{d\gamma}d\gamma. \tag{2.7}$$

Continuity of $s(t)$ in the limit $s \to 0^+$ yields the relation

$$\begin{aligned} s(0) &= \left(s(0) - \frac{r_0}{Eh}p(0)\right)(1 - A_1 - A_2) + \frac{r_0}{Eh}p(0) \\ &= s(0) - \left(s(0) - \frac{r_0}{Eh}p(0)\right)(A_1 + A_2), \end{aligned}$$

giving rise to the constraint that A_1=A_2=0. Hence, an alternative to the extension of (2.4) and (2.5) that is given by (2.7) is now considered.

We revise the proposed extended model by adding a new function

$$L(t) = B_1e^{-t/b_1} + B_2e^{-t/b_2}$$

to the term outside the integral. The new extended model is given by

$$s(t) = \left(s(0) - \frac{r_0}{Eh}p(0)\right) L(t) + \frac{r_0}{Eh}p(0) + \frac{r_0}{Eh}\int_0^t G(t-\gamma)\frac{dp}{d\gamma}d\gamma.$$

Continuity of $s(t)$ in the limit $t \to 0^+$ yields the relation

$$s(0) = \left(s(0) - \frac{r_0}{Eh}p(0)\right)(B_1 + B_2) + \frac{r_0}{Eh}p(0).$$

This gives rise to the new constraint

$$B_1 + B_2 = 1 \qquad \Rightarrow \qquad B_2 = 1 - B_1.$$

Thus, the extended model simplifies to

$$\begin{aligned} s(t) = &\left(s(0) - \frac{r_0}{Eh}p(0)\right)\left(B_1 e^{-t/b_1} + (1-B_1)e^{-t/b_2}\right) + \frac{r_0}{Eh}p(0) \\ &+ \frac{r_0}{Eh}\int_0^t \left[1 - A_1 e^{-(t-\gamma)/b_1} - A_2 e^{-(t-\gamma)/b_2}\right]\frac{dp}{d\gamma}d\gamma. \end{aligned} \tag{2.8}$$

We note that this model can be reduced to the Kelvin model, i.e., (2.4) and (2.5), in the special case

$$B_1 = 1, \;\; A_1 = \frac{\tau_\sigma - \tau_\epsilon}{\tau_\sigma}, \;\; A_2 = 0, \;\; b_1 = \tau_\sigma, \;\; b_2 \;\text{ arbitrary.} \tag{2.9}$$

We remark that our extended model can be viewed as an extension of the Kelvin model to permit multiple relaxation times $b_1, b_2, ...$, to improve the approximation to either the Fung QLV kernel model or the internal strain variable approach of [5–7], each of which permit a continuum of relaxation times in generalized viscoelastic formulations.

2.3 Parameter estimation

Similar to the efforts in our previous study [22], we used pressure as an input to predict cross-sectional area of the vessel. Also, similar to our previous study [22] we re-wrote the model (2.8) using integration-by-parts to avoid using the derivative of pressure as an input. Thus, we obtained

$$\begin{aligned} s(t) = &\left(s(0) - \frac{r_0}{Eh}p(0)\right)\left(B_1 e^{-t/b_1} + (1-B_1)e^{-t/b_2}\right) \\ &+ \frac{r_0}{Eh}p(t)\left(1 - A_1 - A_2\right) + \frac{r_0}{Eh}p(0)\left(A_1 e^{-t/b_1} + A_2 e^{-t/b_2}\right) \\ &+ \frac{A_1}{b_1}\frac{r_0}{Eh}\int_0^t e^{-(t-\gamma)/b_1}p(\gamma)d\gamma + \frac{A_2}{b_2}\frac{r_0}{Eh}\int_0^t e^{-(t-\gamma)/b_2}p(\gamma)d\gamma. \end{aligned} \tag{2.10}$$

For convenience the relations for A_1 and b_1 in (2.9) are substituted into (2.10) prior to data analysis. Consequently, the four independent parameters in the Kelvin model (2.5), $\theta_K=\{r_0, Eh, \tau_\sigma, \tau_\epsilon\}$ are contained in the set of the 7 independent parameters of the extended viscoelastic model (2.10), $\theta_E=\{\theta_K; b_2, A_2, B_1\}$.

The models presented in this study have been validated using in-vitro experimental data that mimic the in-vivo hemodynamic conditions in Merino sheep. The data include in-vitro measurements of blood pressure p_j and vessel diameter D_j. Cross-sectional area is obtained from the diameter measurements by $a_j=\pi(D_j/2)^2$. Note, in the following we treat the extracted cross-sectional areas as data. Both time series were measured under physiological flow, pressure, and stretch conditions with a sampling rate of 200 Hz. During experiments, the vessel segments were mounted in a mock circulation system, and a pulse wave generated by an artificial Jarvik heart was propagated through the system. The frequency of the pulse waves was set to mimic the heart rate of a sheep. In this study, data from one sheep from two vessels (the aorta and the carotid artery) were analyzed. Location of these vessels are shown in Fig. 2. Details of the experimental protocol can be found in [1, 18, 19, 22].

The two models (the Kelvin model and the extended viscoelastic model) were analyzed via solution of the associated inverse problem. Solution of the inverse problem aims at selection of a set of parameters from a set of initial parameters using techniques from nonlinear optimization that allow estimation of model parameters by minimizing the difference between computed and measured quantities. In this study, we estimated model parameters (using blood pressure as an input) by minimizing the difference between computed and measured values of cross-sectional area. To set up the inverse problem we used values from Fung's work [12] to get a initial parameter value for elastic modulus E. Initial parameter values for the wall-thickness h and the unstressed vessel radius r_0 were obtained from the experimental procedure as described by Valdez-Jasso et al., [22]. Initial values for the relaxation times were estimated and set such that they were an order of magnitude apart. For the extended viscoelastic model, we used optimized values from the Kelvin model as initial parameter estimates. Initial parameter values are given in Table 1. To solve the nonlinear inverse problem we used the Nelder-Mead method (a simplex method) as implemented in the Matlab function *fminsearch*.

2.4 Statistical model

Given that the data set predicting vessel area contains n scalar observations, we assume that the statistical model can be written as

$$\tilde{Y}_j = A_j(\theta) + A_j(\theta)^\rho \epsilon_j, \quad j = 1, 2, ...n, \tag{2.11}$$

where $A_j=A(t_j, \theta)$ is the model evaluated at times t_j for each observation obtained from the strain-cross-sectional area relation presented in (2.1), $\theta \in \mathcal{R}^{n_p}$, where n_p is the size of the set of theoretical true parameter values for the model $A(t)$ and ρ is

a non-negative real value. Furthermore, it is assumed that the measurement errors $\epsilon_j, j=1,2,...,n$, are independent identically distributed $(i.i.d.)$ random variables with mean $E[\epsilon_j]=0$ and constant variance $var[\epsilon_j]=\sigma_0^2$, where σ_0^2 is unknown.

The statistical model (2.11) dictates use of ordinary least squares (OLS) when $\rho=0$ and for any other values of ρ it suggests use of generalized least squares (GLS). The two cases of GLS studied here were $\rho=0.5$ and $\rho=1$ [2,9].

An iterative approach is needed for implementing the GLS method. The first iterate $\theta^{(0)}$ uses the set of optimized parameters $\hat{\theta}$ found using OLS (with the weight $w=1$ and $\rho=0$). Given the k^{th} iterate $\theta^{(k)}$, to generate the $(k+1)^{st}$ iterate, we calculated the weights, $w_j^{(k)}=1/A_j(\theta^{(k)})^{2\rho}$, for a fixed value of ρ (equal to either 0.5 and 1). Once the weight was calculated, the corresponding weight was included in the error term $\sum_j^n w_j^{(k)}|A_j(\theta)-a_j|^2$, which is then minimized over θ to obtain $\theta^{(k+1)}$. This iterative procedure was continued until the standard error was constant [2,8,9].

In addition to analyzing the Kelvin model via solution of the GLS, we compared the Kelvin model and the extended model using statistical comparison techniques, which provide quantitative measures of the results. The model comparison is carried out using generalized analysis of variance type statistical tests that involve the residual sums of squares. Since the Kelvin model involves a restricted parameter set in the space of parameters for the extended model, the extended model reduces to the Kelvin model when θ is restricted to $\Theta_H=\{\theta\in\Theta|H\theta=\text{constant}\}$, where H, a (3×4) matrix of rank $r=3$, and the constant are given by

$$\begin{pmatrix} 0 & 1 & 0 & 0 \\ 0 & 0 & 1 & 0 \\ 0 & 0 & 0 & 1 \end{pmatrix} \begin{pmatrix} \theta_k \\ b_2 \\ A_2 \\ B_1 \end{pmatrix} = \begin{pmatrix} 1 \\ 0 \\ 1 \end{pmatrix}.$$

Thus, to compare the models we tested the null hypothesis $H_0 : \theta_E \in \Theta_H$.

In order to test the significance of extending the Kelvin model by including additional relaxation times, we used the error terms computed via solution of the OLS of

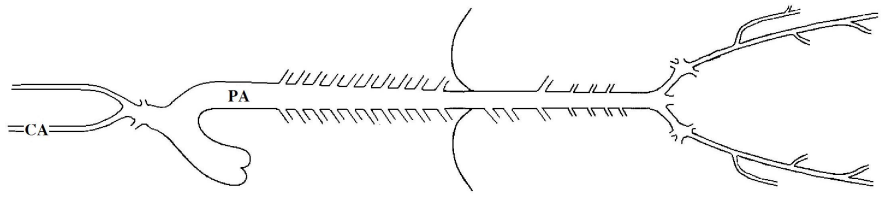

Figure 2: Sketch of the major ovine arteries. Experimental measurements p_j of pressure and cross-sectional area a_j are obtained from the thoracic descending aorta marked by (PA) and from the carotid artery marked by (CA).

the Kelvin and the extended models, and define a test statistic

$$U_n = n\frac{J_K(\theta_K) - J_E(\theta_E)}{J_E(\theta_E)}, \tag{2.12}$$

which under conditions similar to those in an asymptotic sampling distribution theory [2–4, 8], converges as $n\to\infty$ to a random variable with a $\chi^2(r)$ distribution, where r is the difference in degrees of freedom of the two models. In this case we can use the $\chi^2(3)$ distribution to test our hypothesis: if the corresponding test statistic realization $\hat{U}_n$ is greater than $\bar{\tau}$, where $\bar{\tau}$ is a critical value associated with some specific $1-\alpha$ confidence level, then we reject H_0 (i.e., reject the Kelvin model). Otherwise, we cannot reject H_0. Rejection of H_0 suggests statistically that the extended model is an improved description of the data. Given a 95% confidence level, the $\bar{\tau}$ critical value for α=0.05 is $\bar{\tau}$=7.814 (see `http://www.statsoft.com` for $\chi^2(3)$ tables). Here we test the probability $P(U_n>\bar{\tau})=\alpha$. Illustrative examples using this model comparison methodology can be found in Chapter 5 of [4] and Chapter 3 of [8].

3 Results

3.1 Optimization results

As described above, we used the Nelder-Mead method to determine a set of parameters that minimize the OLS error between the computed and measured values of cross-sectional area. The OLS error is given by

$$J(\theta) = \frac{1}{n}\sum_{j}^{n} |A_j(\theta) - a_j|^2,$$

where a_j is the measured cross-sectional area data, $A_j(\theta)=A(t_j,\theta)$ are the computed model values of the cross-sectional area for given parameter values θ, and n is the number of observations. We optimize $J(\theta)$ to obtain the OLS parameter estimates $\hat{\theta}$, resulting in the parameter values given in Table 1.

We also carried out the inverse problems for both models using GLS optimization criteria. Fig. 3 depicts the GLS residuals computed using the Kelvin model with ρ=1. Results are predicted for both the thoracic descending aorta (top graphs) and the carotid artery (bottom graphs). Results suggest that our assumption of constant variance may fail for both vessels (i.e., both data sets). Nonetheless, we perform a comparison of the two models and their relative reduction in residuals for the OLS determined parameters of Table 1.

3.2 Uncertainty analysis

After carrying out the optimizations and obtaining the results reported in Table 1, we computed the relevant realizations for the test statistics as defined in (2.12). For the

Table 1: Initial and optimized parameter values for the Kelvin model and the extended viscoelastic model for the thoracic descending aorta and the carotid artery.

		Thoracic descending aorta				**Carotid artery**			
		Kelvin		Extended		Kelvin		Extended	
		Init	Opt ($\hat{\theta}_K$)	Init	Opt ($\hat{\theta}_E$)	Init	Opt ($\hat{\theta}_K$)	Init	Opt ($\hat{\theta}_E$)
r_0	cm	0.93	0.86	0.86	0.86	0.45	0.44	0.44	0.45
Eh	mmHg cm	234	669	669	659	203	1505	1505	2604
$\tau_\sigma \times 10^2$	sec	5.00	5.94			5.00	44.5		
$\tau_\epsilon \times 10^2$	sec	2.50	2.96			2.50	13.7		
A_1				0.50	0.48			0.50	0.35
A_2				0.50	0*			0.50	0.44
$b_1 \times 10^2$	sec			5.00	6.64			5.00	44.4
$b_2 \times 10^2$	sec			2.50	4.80			2.50	3.51
B_1				0.50	0*			0.50	0*
$J \times 10^7$			13400		13200		2.92		1.73

thoracic descending aorta, we find $J_K(\hat{\theta}_K)$=13400 $\times$ 10^{-7} and $J_E(\hat{\theta}_E)$=13200 $\times$ 10^{-7}. For this data set we had n=302 so using (2.12) we obtain the test statistic

$$\hat{U}_n = n\frac{J_K(\hat{\theta}_K) - J_E(\hat{\theta}_E)}{J_E(\hat{\theta}_E)} = 4.58.$$

Thus for the thoracic descending aorta we conclude that inclusion of more relaxation times (use of the extended model) does not provide a statistically significant improvement over the Kelvin model (at the 95% confidence level, where $\bar{\tau}$=7.814). Using a similar calculation for the carotid artery (the data in this case was for n=335), we found $\hat{U}_n$=230.43. Thus, for the carotid artery data, the inclusion of an additional relaxation time provides a statistically significantly improved model.

4 Discussion

This study demonstrates that both the Kelvin and the extended models are able to predict viscoelastic features of the vessel wall deformation under in-vitro conditions that mimic physiological flow, pressure, and stretch. Prediction of elastic modulus times wall thickness Eh shows that the aorta is significantly less stiff than the carotid artery, i.e., $Eh_{aorta} \ll Eh_{carotid}$ (see Table 1). In addition, we observe that one of the relaxation time scales is an order of magnitude larger for the carotid artery than for the aorta. This is confirmed by computing the phase-shift. For the Kelvin model the phase-shift can be predicted by

$$\tan(\delta) = \frac{\omega(\tau_\sigma - \tau_\epsilon)}{1 + \omega^2\tau_\sigma\tau_\epsilon}, \quad \omega = \frac{2\pi}{T},$$

where ω 1/sec is the frequency and T sec is the length of the cardiac cycle. It should be noted that this equation is derived to study phase shifts of a pure harmonic wave,

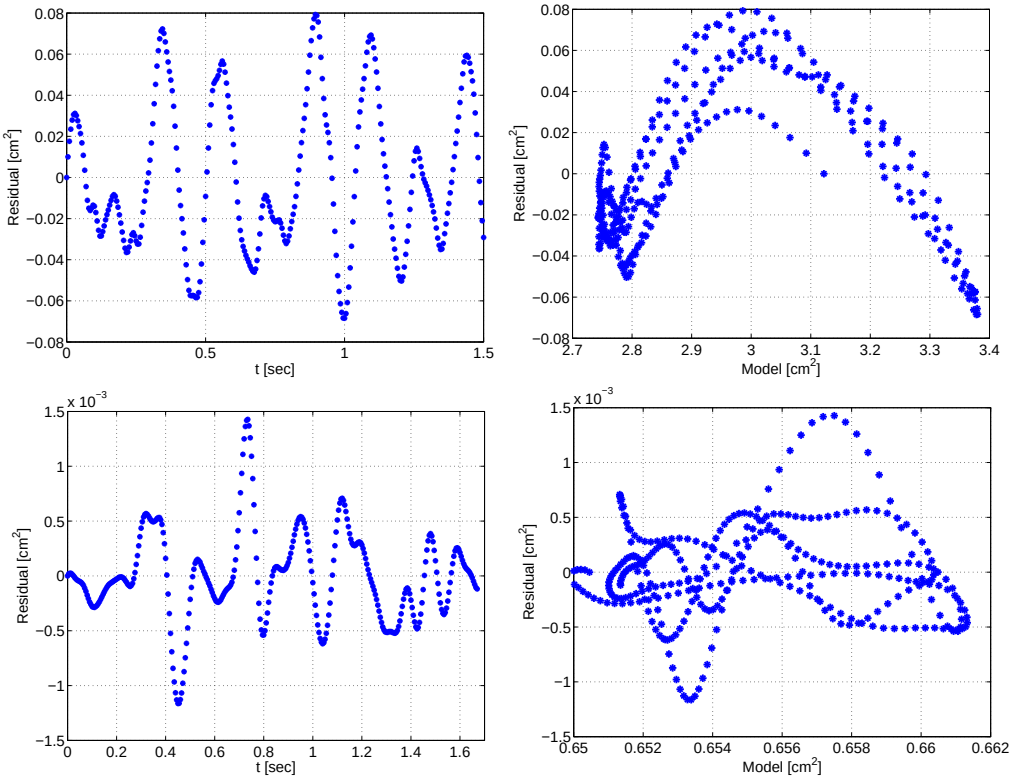

Figure 3: Results from the GLS using thoracic descending aorta (first row) and carotid artery (second row), both presenting the case when ρ=1. Left column shows the residual r_j=$(a_j - A_j(\hat{\theta}))/A_j(\hat{\theta})$ as a function of time, and the right column shows the residual as a function of the model. Results from other values of ρ (not shown) looked similar.

and in our study the pressure waves propagating along the vessels are composed of multiple frequencies. For the Kelvin model, the phase-shift δ=15.8 degrees for the thoracic descending aorta and δ=21.3 degrees for the carotid artery. These results confirm the biological notion that the carotid artery is more viscoelastic than the aorta. This agrees with the histological observation that the viscoelastic smooth muscle cells are more abundant in the carotid artery than in the thoracic descending aorta [15].

In addition to these components, the aorta also contains fibers supporting the vessel wall and cells aligned in a helix [20]. Furthermore, the adventitia may have a more prominent role in the aorta than in the smaller arteries [10]. As a result, the aorta exhibits a more complex "nonlinear" stiffening, evidenced by decreasing slope of the pressure-area curve as pressure increases. This can be seen by analyzing the hysteresis loops shown in Fig. 5 (right column).

Note how the upper part of the pressure-area curve representing the relaxation phase of the cardiac cycle changes slope for the aorta, while the carotid artery does not display these dynamics. Consequently, neither the Kelvin model nor the extended model is capable of adequately reproducing this important component of the mechan-

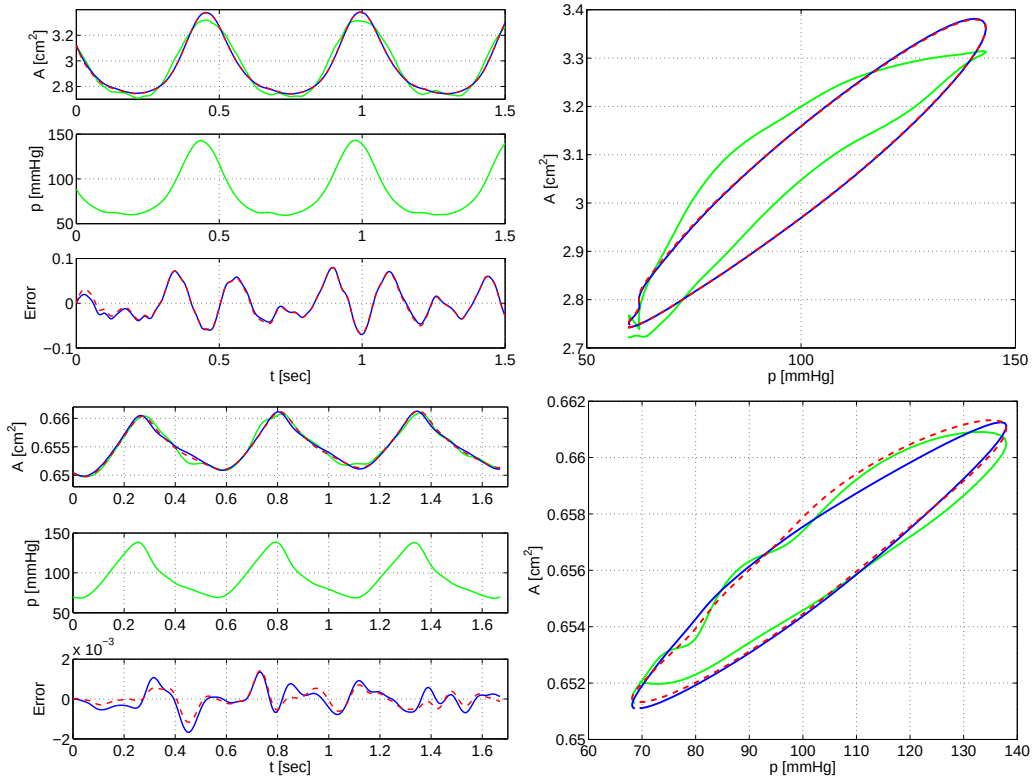

Figure 4: Results from the thoracic descending aorta (top graphs) and carotid artery (bottom graphs) comparing the Kelvin model (dark line) and the extended model (dashed line) using pressure data (gray line) as an input to predict vessel area data (gray line). The left panels show vessel area as a function of time, blood pressure (input), and the error between computed $A_j(\theta)$ and measured a_j areas. The right column shows relation between pressure and area for one cycle from the thoracic descending aorta (top graph) and from the carotid artery (bottom graph).

ical deformation for the thoracic descending aorta data. This is also confirmed by the statistical tests used to compare the models, which showed that the two models cannot be distinguished for the aorta. The carotid artery does not display significant nonlinear stiffening, but it displays significant viscoelastic damping. Consequently, for this vessel our statistical analysis confirmed that the extended model improves predictions of the vessel deformation. The latter can also be observed by the improved fit to the pressure-area data for the carotid artery, i.e., J=1.73 $\times$ 10^{-7} for the extended model versus J=2.92 $\times$ 10^{-7} for the Kelvin model (see Table 1).

These findings are in agreement with previous studies, e.g., Kassab [14] and Schulze-Bauer and Holzapfel [21], which suggest that hyperelastic models are more appropriate for predicting elastic deformation of the aorta. As such, future studies by our group are considering development of nonlinear extensions to the linear viscoelastic models described above.

Another question to be addressed in future studies relates to the observation that, for the extended model, our calculations (not presented here) reveal that the parame-

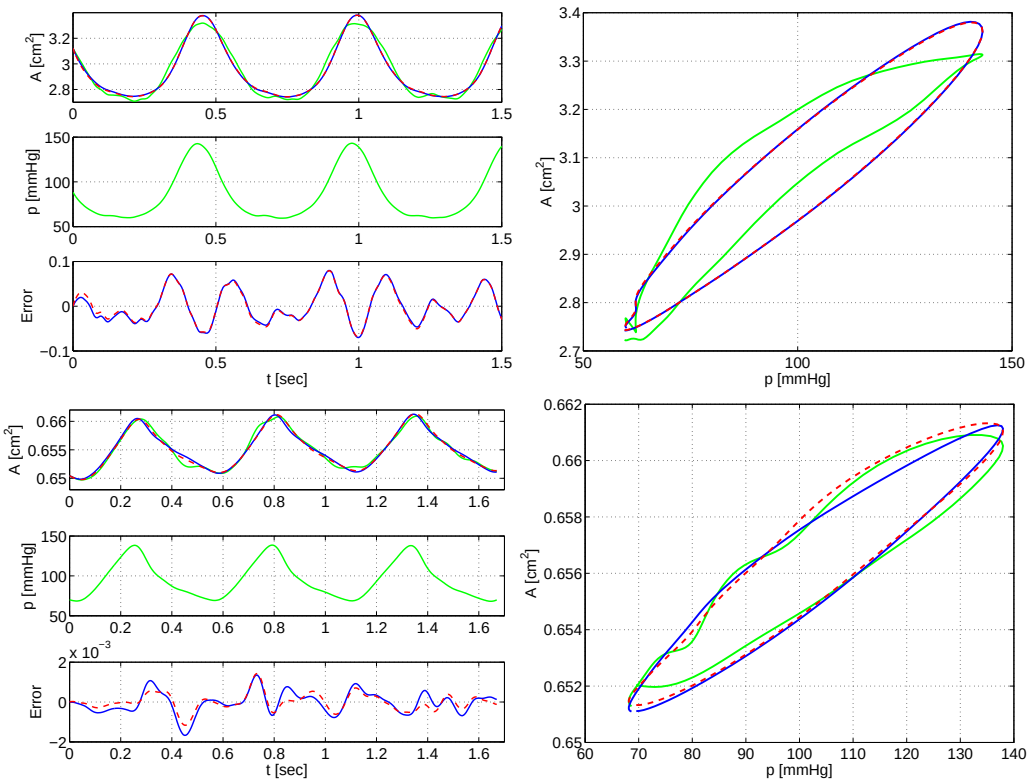

Figure 5: Results from the thoracic descending aorta (top graphs) and carotid artery (bottom graphs) comparing the Kelvin model (dark line) and the extended model (dashed line) using pressure data (gray line) as an input to predict vessel area data (gray line). The left panels show vessel area as a function of time, blood pressure (input), and the error between computed $A_j(\theta)$ and measured a_j areas. The right column shows relation between pressure and area for one cycle from the thoracic descending aorta (top graph) and from the carotid artery (bottom graph).

ters are correlated and solutions to the inverse problem only ensures a local minimum. For the Kelvin model, parameters are not correlated and solutions to the inverse problem always gave the same set of parameters, even when initial parameter values for optimization were varied by several orders of magnitude. Preliminary results with the extended model showed that even small variations in initial parameter values gave rise to significant changes in the optimized parameter values, without changing the end cost. In particular, we observed that values for B_1 tend to switch between positive values close to zero and larger than 1, giving rise to a switch in the roles of the two relaxation factors. One way to avoid this kind of behavior is to enforce more constraints on the model parameters, e.g., one could enforce $B_1 \ll 1$. Another option is to use sensitivity analysis combined with subset selection to estimate a reduced set of parameters to be optimized. Such techniques have been used successfully in previous studies, see e.g., [17]. In this study the goal was to compare the two models to test if the extended model is more accurate; thus the parameter uniqueness question is not addressed here. We remark that if the model is to be used for analysis of large data

sets, this question must be addressed before numerous simulations are conducted.

In summary, this study demonstrates the importance of including viscoelasticity when modeling deformation of the large ovine arteries and, in particular, that application of an extended viscoelastic model for the carotid artery significantly improves accuracy over the simpler Kelvin model. On the other hand, for the thoracic descending aorta, it is necessary to develop a more advanced model accounting for nonlinear responses to achieve an improvement in data fitting.

Acknowledgments

This research was supported in part (DVJ) by the Consejo Nacional de Ciencias y Tecnologia de Mexico (CONACYT), in part (HTB) by the US Air Force Office of Scientific Research under grant AFOSR-FA9550-08-1-0147 and by the National Institute of Allergy and Infectious Disease under grant NIAID 9R01AI071915-05, in part (MAH) by the National Science Foundation under grant DMS-0636590 and by the National Institutes of Health under grant NIH-AG-15768, and in part (MSO) by the National Science Foundation under grant DMS-0616597. In addition, Drs. Bia, Zocalo and Armentano would like to thank Mr. Juan D. Fernandez and Ms. Paula Bia for their contribution with the histological studies and the process of the histological images, respectively.

References

[1] R.L. ARMENTANO, J.G. BARRA, F.M. PESSANA, D.O. CRAIEM, S. GRAF, D. BIA SANTANA AND R.A. SANCHEZ, *Smart smooth muscle spring-dampers. Smooth muscle smart filtering helps to more efficiently protect the arterial wall,*, IEEE Engr Med Biol Mag., 26 (2007), pp. 62-70.

[2] H.T. BANKS, M. DAVIDIAN, J. SAMUELS AND K. SUTTON,, *An inverse problem statistical methodology summary,* CRSC Tech Report, CRSC-TR08-01, NCSU, January, 2008; in Statistical Estimation Approaches in Epidemiology, (edited by Gerardo Chowell, Mac Hyman, Nick Hengartner, Luis M.A Bettencourt and Carlos Castillo-Chavez), Springer, Berlin Heidelberg New York, to appear.

[3] H. T. BANKS AND B. G. FITZPATRICK, *Statistical methods for model comparison in parameter estimation problems for distributed systems*, CAMS Tech. Rep. 89-4, September, 1989, University of Southern California; J. Math. Biol., 28 (1990), pp. 501–527.

[4] H. T. BANKS AND K. KUNISCH, *Estimation Techniques for Distributed Parameter Systems*, Birkhaüser, Boston, 1989.

[5] H. T. BANKS, N. MEDHIN, AND G. A. PINTER, *Multiscale considerations in modeling of nonlinear elastomers*, International Journal for Computational Methods in Engineering Science and Mechanics, 8 (2007), pp. 53-62.

[6] H. T. BANKS AND G. A. PINTER, *A probabilistic multiscale approach to hysteresis in shear wave propagation in biotissue*, CRSC-TR04-03, NCSU, January, 2004; SIAM J. Multiscale Modeling and Simulation, 2 (2005), pp. 395-412.

[7] H. T. BANKS AND J. R. SAMUELS, *Detection of cardiac occlusions using viscoelastic wave propagation*, Advances in Applied Mathematics and Mechanics, to appear.

[8] H. T. BANKS AND H. T. TRAN, *Mathematical and Experimental Modeling of Physical and Biological Processes*, Chapman & Hall/CRC Press, Boca Raton, FL, 2009.
[9] M. DAVIDIAN AND D. GILTINAN, *Nonlinear Models for Repeated Measurements Data. Monographs on Statistics and Applied Probability 62*, Chapman & Hall/CRC Press, Boca Raton, FL, 1998.
[10] E. I. C. FISHER, D. BIA AND J. CAMUS, R. A. Y. ZOCALO AND R. L. E. DE FORTEZA, *Adventitia-dependent mechanical properties of brachiocephalic ovine arteries in in-vivo and in-vitro studies*, Acta Physiol, 188 (2006), pp. 103-111.
[11] Y. C. FUNG, Biomechanics: Mechanical Properties of Living Tissues, Springer Verlag, New York, 1993.
[12] Y. C. FUNG, Biomechanics: Circulation, Springer Verlag, New York, 1996.
[13] R. HOLENSTEIN AND P. NIEDERER, *A viscoelastic model for use in predicting arterial pulse waves*, J Biomech Engr., 102 (1980), pp. 318-325.
[14] G. S. KASSAB, *Biomechanics of the cardiovascular system: the aorta as an illustratory example*, J. R. Soc Interface, 3 (2006), pp. 719-740.
[15] M. KAWASAKI, Y. ITO, M. ARAI, G. TAKEMURA, A. HARA, Y ICHIKI, H. TAKATSU, S. MINATOGUCHI AND H. FUJIWARA, *Assessment of arterial medial characteristics in human carotid arteries using integrated backscatter ultrasound and its histological implications*, Artherosclerosis, 180 (2005), pp. 145-154.
[16] W. W. NICHOLS AND M. F. O'ROURKE, *Properties of the arterial wall, McDonalds Blood Flow in Arteries*, Theoretical, Experimental and Clinical Principals, Edadrw Arnold, Philadelphia, PA, 1990.
[17] S. R. POPE, L. M. ELLWEIN, C. L. ZAPATA, V. NOVAK, C. T. KELLEY AND M. S. OLUFSEN, *Estimation and identification of paramters in a lumped cerebrovascular model*, Math BioSci Engr, in press (2008).
[18] M. PAGANI, H. BAIG, A. SHERMAN, W.T. MANDERS, P. QUINN, T. PATRICK, D. FRANKLIN AND S.F. VATNER, *Measurement of multiple simultaneous small dimensions and study of arterial pressure-dimension relations in conscious animals*, Am J Physiol, 235 (1978), pp. H1610-H1617.
[19] M. PAGANI, I. MIRSKY, H. BAIG, W. T. MANDERS, P. KERKHOF, AND S. F. VATNER, *Effects of age on aortic pressure-diameter and elastic stiffness-stress relationships in unanestetized sheep*, Circ Res, 44 (1979), pp. 420-429.
[20] J. A. G. RHODIN, Architecture of the Vessel Wall, Handbook of Physiology, Section 2, Volume II, The Cardiovascular System, pp. 1-31, 1980.
[21] C. A. J. SCHULZE-BAUER AND G. A. HOLZAPFEL, *Determination of constitutive equations for human arteries from clinical data*, J Biomech, 36 (2003), pp. 165-169.
[22] D. VALDEZ-JASSO, M. A. HAIDER, H. T. BANKS, D. BIA, Y. ZOCALO, R. L. ARMENTANO AND M. S. OLUFSEN, *Analysis of viscoelastic wall properties in ovine arteries*, IEEE Trans Biomed Engr, forthcomming article, 2008. DOI:10.1109/TBME.2008.2003093
[23] R. P. VITO AND S. A. DIXON, *Blood vessel constitutive models* 1995-2002, Ann Rev Biomed Engr, 5 (2003), pp. 413-439.
[24] W. ZHANG, H. CHEN AND G. KASSAB, *A rate-insensitive linear viscoelastic model for soft tissues*, Biomaterials, 28 (2007), pp. 3579-3586.